Design and Implementation of a Multi-Purpose TMR Sensor Matrix for Wireless Electric Vehicle Charging

Xuyang Liu, *Student Member, IEEE*, Chunhua Liu, *Senior Member, IEEE*, Wei Han, *Student Member, IEEE*, and Philip W. T. Pong, *Senior Member, IEEE*

***Abstract*— A cost-effective technology to monitor the charging performance and detect the coil misalignment and foreign metal objects is indispensable to the commercialization of wireless power transfer on electric vehicle (EV) charging. This paper presents a multi-purpose tunneling magnetoresistive (TMR) sensor matrix, which can monitor the charging performance as well as detect both the coil misalignment and metal objects for wireless EV charging. The magnetic field distribution between coils is measured by the TMR sensor matrix to provide the critical information about charging performance, coil misalignment position, and the existence of metal objects. The mutual inductance and charging power are derived from the measured z-components of the magnetic flux densities. Lateral misalignment position is determined by the symmetry coefficients of the time-varying magnetic field distribution in the range of ±150 mm. Metal objects are detected by the measured magnetic field offsets. In this paper, both 3D finite-element-method modeling and experimental results were presented to demonstrate the effectiveness of the proposed approach. A 14 × 14 TMR sensor matrix with high sensitivity of 80 mV/V/mT was designed and implemented to measure the magnetic field distribution in order to demonstrate the technology.**

***Index Terms*— Tunneling magnetoresistive (TMR) sensors, sensor matrix, wireless power transfer (WPT), electric vehicle (EV) charging, coil misalignment detection, foreign metal object detection.**

I. Introduction

WIRELESS power transfer (WPT) technology has been applied in a wide range of commercial products, such as mobile phone devices, biomedical electronics and industrial devices [1]. Inductive coupling WPT technology can transfer power to electric vehicles (EVs) over a relatively long distance at the kilowatts power level and thus it can eliminate the inconvenient wiring [2]–[4]. The vehicle-mounted receiver initiates charging while the EV is parked above the ground-embedded transmitter. However, the stationary wireless EV charging still suffers from the following issues before their commercialization:

1) Monitoring the charging performance in a convenient way;
2) Detecting the lateral misalignment between coils;
3) Detecting the foreign metal objects between the transmitter and receiver.

Traditionally, the charging performance of the wireless charging system is monitored by measuring both the mutual inductance and transferred power [5]. The transferred power can be measured from the receiver side while the mutual inductance needs to be measured from both the transmitter and receiver sides [6]. Thus, it is inconvenient to find out the mutual inductance in an operating wireless charging system.

Both the transferred power and charging efficiency of wireless charging system are sensitive to the positions of the transmitting and receiving coils. The coil misalignment leads to the significant reduction of transferred power and charging efficiency. Researchers have made progress on improving the coil misalignment for wireless EV charging [7]–[11]. Wireless radio sensors were installed on the coils to measure the distances and then detect the misalignment with relatively high accuracy [7]. However, this misalignment detection relies on the complex and time-consuming computation algorithm. On the other hand, magnetic misalignment detection by means of search coils or auxiliary coils has also been introduced [8]–[11], which uses the existing charging facility. However, these sensing coils are limited by their relatively bulky size and the difficulty of replacing faulty coils for maintenance and repair.

Meanwhile, foreign objects of ferrous materials between the transmitter and receiver need to be detected during the charging operation to prevent heating or combustion of the metallic object due to the eddy current losses. Several metal object detection methods have been introduced by means of measuring power losses [12], the quality factor of the secondary coil [13] and the impedance of the transmitting coil [14]. However, these methods are confined to only the WPT applications where the coils positions are fixed. Another metal object detection method measures the magnetic field

Manuscript received September 10, 2018; revised October 27, 2018; accepted November 20, 2018. Date of publication November 28, 2018; date of current version February 6, 2019. This work was supported in part by the Seed Funding Program for Basic Research, in part by the Seed Funding Program for Applied Research and Small Project Funding Program from The University of Hong Kong, in part by the ITF Tier 3 funding under Grant ITS/203/14, Grant ITS/104/13, and Grant ITS/214/14, in part by the RGC-GRF Grant HKU 17210014 and Grant HKU 17204617, and in part by the University Grants Committee of Hong Kong under Contract AoE/P-04/08. The associate editor coordinating the review of this paper and approving it for publication was Prof. Nitaigour P. Mahalik. *(Corresponding author: Philip W. T. Pong.)*

X. Liu, W. Han, and P. W. T. Pong are with the Department of Electrical and Electronic Engineering, The University of Hong Kong, Hong Kong (e-mail: ppong@eee.hku.hk).

C. Liu is with the School of Energy and Environment, City University of Hong Kong, Hong Kong.

Digital Object Identifier 10.1109/JSEN.2018.2883708

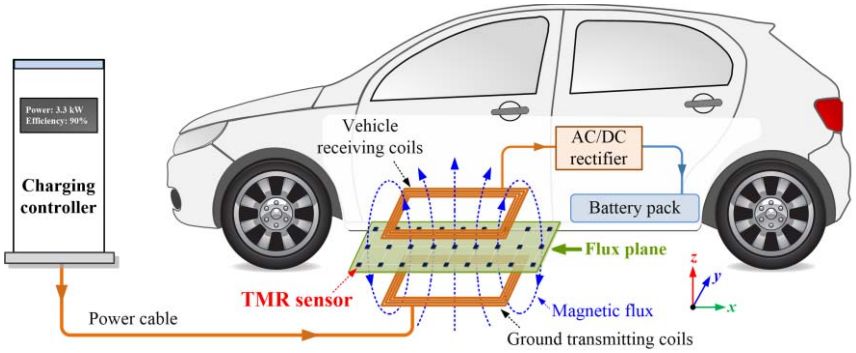

Fig. 1. Conceptual diagram of the multi-purpose TMR sensor matrix for wireless charging of EVs.

generated from the metallic magnetic objects by using the nonoverlapping coil sets [15]. However, the implementation and maintenance of the coils sets are too complicated in the practical EV charging applications.

In this paper, a new multi-purpose approach to achieve the charging performance monitoring, lateral coil-misalignment detection and foreign metal object detection for wireless charging EVs using a tunneling magnetoresistive (TMR) sensor matrix is proposed and tested. Comparing to the previous work that focuses on the one-dimensional lateral coil-misalignment detection using a TMR sensor array [16], in this work the magnetic field distribution between the ground-embedded transmitting coils and vehicle-mounted receiving coils provides multiple information of the wireless charging performance, two-dimensional coil-misalignment position, and existence of metal objects. The sensitive TMR sensor matrix mounted below the receiving coil is capable of measuring both the time-varying and constant magnetic field to achieve three purposes: charging performance monitoring, two-dimensional lateral misalignment detection and foreign metal object detection. The advantages such as low cost, high sensitivity, low power consumption and large measuring range make TMR sensors well qualified in wireless charging EVs applications [17]–[19]. The compact-in-size TMR sensors can be mounted on the printed circuit boards (PCBs), which make the installation and maintenance of sensor matrix much easier than the nonoverlapping coil sets.

This paper is organized as follows. Section II provides the working principle of multi-purpose TMR sensor matrix for monitoring charging performance and detecting coil misalignment and foreign metal objects for stationary wireless EV charging. A 3D finite-element-method (FEM) modeling was carried out to validate the proposed approach which is discussed in Section III. Section IV describes the experiments that includes the implementation of the sensor matrix, experimental setup, and the pre-calibration of the sensor matrix. Section V presents the experimental results that demonstrate the effectiveness of the proposed approach. Section VI finally addresses the conclusion of this work.

II. Working Principle

This section reveals the basic operating principle of the multi-purpose TMR sensor matrix for the stationary wireless

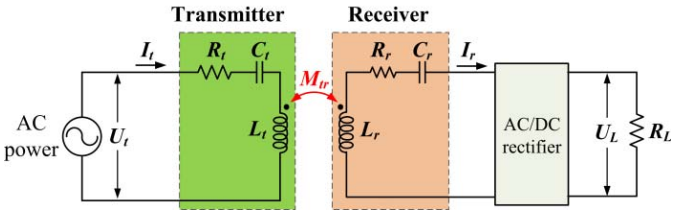

Fig. 2. Schematic view of the IPT-based WPT system.

EV charging. Fig. 1 depicts the conceptual diagram of the TMR sensor matrix configuration for wireless EV charging. The stationary charging controller that connects to the power grid can provide AC power to the ground transmitting coils. Energy is wirelessly transferred through the inductive power transfer (IPT) mechanism when the ground transmitting coils and vehicle receiving coils are in resonance. The resonance frequency of the transmitting and receiving coils is the same (i.e., typically 10∼100 kHz) [20]. The transferred power is then applied to charge the EV batteries using the AC/DC rectifier and regulator. In this work, the TMR sensor matrix is placed below the vehicle receiving coil to measure the magnetic flux density distribution, which provides the critical information on charging performance, coil misalignment positions and the existence of metal objects.

A. Charging Performance Monitoring

The mutual inductance and transferred power are the key parameters determining the charging performance for wireless EV charging. Fig. 2 shows the IPT-based WPT system that adopts series-series topology, which comprises of the transmitter unit and the receiver unit. The loop impedances of the transmitter (Z_t) and the receiver (Z_r) can be calculated by:

$$Z_t = R_t + \frac{1}{j\omega C_t} + j\omega L_t \tag{1}$$

$$Z_r = R_L + R_r + \frac{1}{j\omega C_r} + j\omega L_r \tag{2}$$

where R_t and R_r are the internal resistances of the transmitting and receiving coils, respectively, R_L is the load resistance, L_t and L_r are the inductances of the transmitting and receiving coils, respectively, C_t and C_r are the compensation capacitors

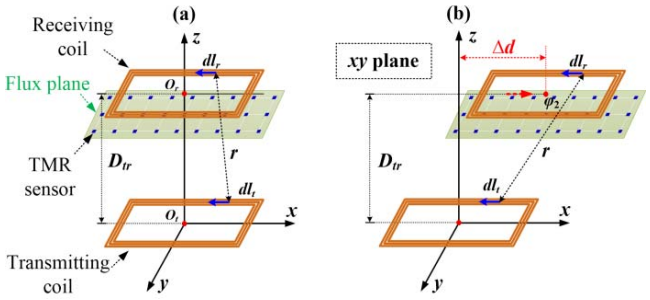

Fig. 3. 3-D geometry of coil configurations in WPT: (a) well-alignment and (b) lateral misalignment.

of the transmitter and receiver unit, respectively, and ω is the resonance frequency.

The transferred power (P_L) and the real power transfer efficiency (η) can be calculated by [21]:

$$P_L = \mathrm{Re}[V_L \cdot I_r^*] = \frac{\omega^2 M_{tr}^2 \cdot R_L \cdot I_t \cdot I_t^*}{Z_r \cdot Z_r^*} \tag{3}$$

$$\eta = \frac{\mathrm{Re}[V_L \cdot I_r^*]}{\mathrm{Re}[V_T \cdot I_t^*]} = \frac{\omega^2 M_{tr}^2 \cdot R_L}{\mathrm{Re}[Z_T \cdot Z_R \cdot Z_R^* + \omega^2 M_{tr}^2 \cdot Z_R^*]} \tag{4}$$

where M_{tr} is the mutual inductance, and I_t and I_r are the currents through the transmitting and receiving coils, respectively. Assuming that the constant current (I_t) power supply and fixed load (R_L) are used in wireless charging, both P_L and η can be found out by the value of M_{tr}.

According to the double integral Neumann formula [6] (see Fig. 3(a)), M_{tr} can be determined by

$$M_{tr} = \frac{\mu_0}{4\pi} \oint_t \oint_r \frac{dl_t dl_r \cos\varepsilon}{D_{tr}} \tag{5}$$

where dl_t and dl_r are the infinitesimal segments of the transmitting and receiving coils, respectively, and D_{tr} and ε are the distance and angle between the two coil segments. However, it's impractical to dynamically determine M_{tr} using Eq. (5) in the wireless EV charging applications.

In general, M_{tr} can be defined by

$$M_{tr} = \frac{N_2 \Phi_{21}}{I_t} = \frac{N_2 B A_2}{I_t} \tag{6}$$

where Φ_{21} denotes the magnetic flux through one turn of the receiving coils due to I_t, B is the magnetic flux density, and A_2 is the cross-sectional area of the receiving coils. By utilizing a constant current source (I_t) as the power supply, the magnetic flux across the receiving coils originating from the transmitting coils is directly employed to find out the value of M_{tr}. As the magnetic flux density (B) is dominated by the z-component (B_z) due to the parallel configuration of transmitting and receiving coils, the value of B can be approximated by the value of B_z. Thus, M_{tr} can be computed by

$$M_{tr} \approx \frac{N_2 A_2}{I_t} \oint_s B_z ds \tag{7}$$

An $n \times n$ TMR sensor matrix can be placed under the receiving coils to measure the time-varying z-component of magnetic field. A sensor matrix can provide the magnetic field distribution on the flux plane (see Fig. 3(a)). Thus, M_{tr} is almost proportional to the sum (S_B) of the measured B_z:

$$M_{tr} \propto S_B = \sum_i^n \sum_j^n B_{i,j} \tag{8}$$

Here, $B_{i,j}$ denotes the measured z-component flux density by the sensor at position (i, j) of the sensor matrix. So M_{tr} can be determined using the measured value of S_B by the TMR sensor matrix. In consequence, the transferred power (P_L) can be found according to Eq. (3).

B. Coil-Misalignment Detection

Two types of misalignment including lateral and angular misalignment can exist in WPT [22]. Since angular misalignment is less likely to occur in the practical EV applications [15], [23], this paper only focus on the lateral misalignment detection. The lateral coil misalignment is depicted in Fig. 3(b). Let Δd be the lateral misalignment between the centers of transmitting and receiving coils.

The time-varying magnetic flux through the transmitting and receiving coils can provide the misalignment information between two coils. The lateral coil misalignment leads to the unbalanced magnetic flux distribution on the flux plane. When the receiving coil is well aligned with the transmitting coil, the magnetic flux density distribution across the flux plane is well symmetric and the majority of magnetic flux is at the center position of receiving coil. When there exists a lateral misalignment, the magnetic flux distribution becomes unsymmetrical and the majority of flux shifts according to the misalignment orientations. Thus, it is feasible to use the flux distribution across the receiving coil to detect the misalignment position and orientation.

In this work, two symmetry coefficients (i.e., C_x and C_y) are defined to calculate the flux density symmetry that relates to the coil-misalignment distance and orientation:

$$C_x = \frac{\sum_i \sum_j (B_{n+1-i,j} - B_{i,j})}{S_B} \tag{9}$$

$$C_y = \frac{\sum_i \sum_j (B_{i,n+1-j} - B_{i,j})}{S_B} \tag{10}$$

where C_x and C_y denote the x-axis and y-axis asymmetry coefficients, respectively. When both C_x and C_y are close to zero, the transmitting and receiving coils are well aligned as illustrated in Fig. 3(a). When C_x and C_y are larger than zero, it denotes the coil misalignment along the x-axis and y-axis (Fig. 3(b)), respectively. The misalignment position can also be determined by the values of C_x and C_y.

C. Metal Objects Detection

Metal objects frequently exist between the transmitting and receiving coils in the practical applications, and they absorb the transferred energy due to the eddy currents and possibly become the hazard to the drivers and vehicles. When the metallic object is exposed to the time-varying AC magnetic field (B_{coils}) induced by the coils, eddy current is generated

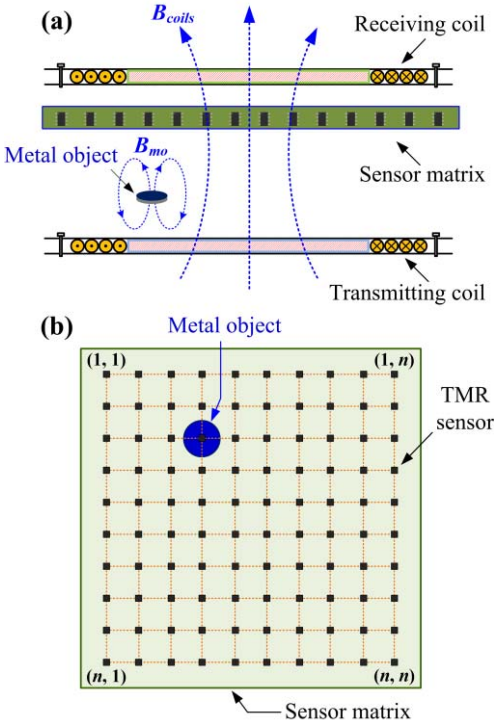

Fig. 4. (a) Side view and (b) top view of metal object detection by TMR sensor matrix.

and an additional magnetic field (B_{mo}) is induced around the metallic object, as shown in Fig. 4(a). Thus, the original magnetic fluxes are distorted by the existence of metallic object. Here, the total magnetic field (B_{tot}) along the sensitive axis of the TMR sensor can be expressed as:

$$B_{tot} = B_{coils} + B_{mo} \tag{11}$$

Typically, B_{mo} is relatively weaker comparing to B_{coils}. The high-sensitive TMR sensor matrix measures B_{tot} over the whole flux plane, and thus the DC magnetic field offsets as well as AC magnetic field distribution can be obtained. The position of magnetic field offset on the flux plane corresponds to the location of the metallic object. Thus, the metallic objects over the transmitting coils can be distinguished and localized by analyzing the voltage outputs of the whole sensor matrix, as illustrated in Fig. 4(b).

III. FEM Modeling

3D FEM simulations of IPT-based WPT were carried out using the commercial simulation software JMAG Designer. The mutual inductance (M_{tr}) and the magnetic flux density distribution on the flux plane between the transmitting and receiving coils were analyzed to validate the proposed multi-purpose approach. The IPT-based WPT with square coil configurations adopting the series-series topology was used in the WPT simulation. The operating frequency of the IPT-based WPT was chosen as 20 kHz. The corresponding key parameters of the IPT-based WPT system are listed in Table I.

By regulating the lateral coil misalignment (Δd) along the x-axis direction, the simulated magnetic flux density distributions under different lateral misalignments were obtained, as illustrated in Fig. 5. It can be observed that the magnetic flux distribution varies in response to the misalignment distance and orientation.

TABLE I
PARAMETERS OF IPT-BASED WPT SYSTEM IN FEM SIMULATIONS

Parameter	Value
Transmitting coil inductance (L_t)	63.26 μH
Transmitting coil internal resistance (R_t)	0.1409 Ω
Transmitting coil number of turns (N_1)	15
Transmitting coil compensation capacitor (C_t)	1.001 μF
Receiving coil inductance (L_r)	63.20 μH
Receiving coil internal resistance (R_r)	0.1399 Ω
Receiving coil number of turns (N_2)	15
Receiving coil compensation capacitor (C_r)	1.002 μF
Current through transmitting coil (I_t)	3~7 A
Load resistance (R_L)	1.0 Ω (50 W)
Operating frequency (f_s)	20 kHz

The simulated coefficient S_B reaches its maximum value when the lateral misalignment (Δd) is zero, as shown in Fig. 6. S_B gradually decreases with the rise of Δd. When Δd reaches 150 mm, the simulated coefficient S_B becomes lower than 5 mT. The WPT models with vertical distances (D_{tr}) of 80 mm and 100 mm show the similar pattern (Fig. 6). Fig. 7 shows the relationship between the mutual inductance (M_{tr}) and the coefficient S_B. It can be observed that M_{tr} is proportional to S_B. A second-order polynomial fit can be applied to well express the relationship between M_{tr} and S_B. Thus, it is feasible to obtain M_{tr} from the measured value of coefficient S_B. Then the transferred power (P_L) can be found from the value of M_{tr} according to Eq. (3).

The simulated symmetry coefficient C_x shows an exponential relationship with the misalignment distance along the x-axis direction, as illustrated in Fig. 8. The WPT models with two vertical distances (i.e., 80 mm and 100 mm) experience the similar pattern. It can be also observed that C_x is independent of the current source. An exponential fit can be applied to express the relationship between the misalignment and the symmetry coefficient (see Fig. 8). Similarly, the symmetry coefficient C_y also shows the exponential relationship with the misalignment distance along the y-axis direction. Thus, the misalignment distance and orientation can be detected by the measured symmetry coefficients.

The FEM simulations for the foreign metal object detection were also carried out in this work. The simulation results show that the metal object inserted in between the coils induces an additional constant DC magnetic field, which leads to the offset of the magnetic flux density distribution. Fig. 9 (a) and Fig. 9(b) show the simulated magnetic flux density distributions when a metallic object of round steel sheet (with radius of 10 mm) exists at the positions of (0 mm, 0 mm) and (−30 mm, −30 mm), respectively. The vertical distance between the metal object and receiving coil is 50 mm. The metal object can be distinguished by the region of large offsets. The region of magnetic field offsets depends on both

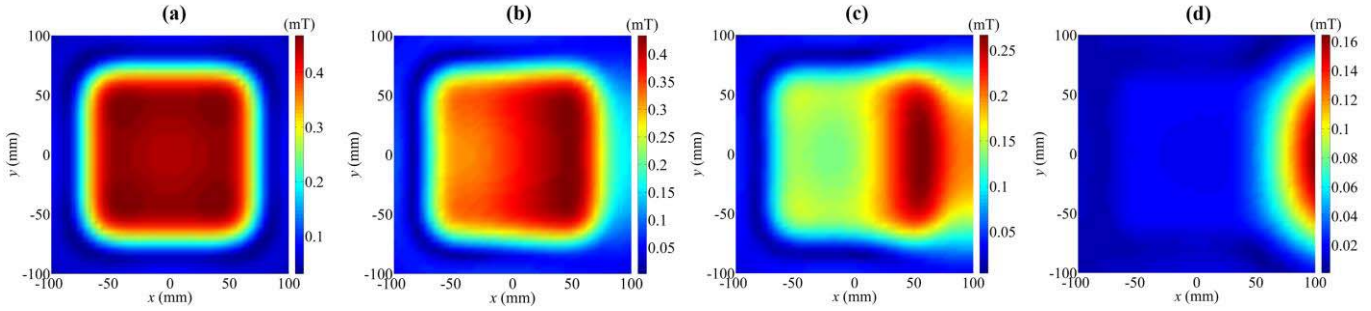

Fig. 5. Simulated magnetic field distributions under lateral misalignments: (a) $\Delta d = 0$ mm, (b) $\Delta d = 50$ mm, (c) $\Delta d = 100$ mm, and (d) $\Delta d = 150$ mm.

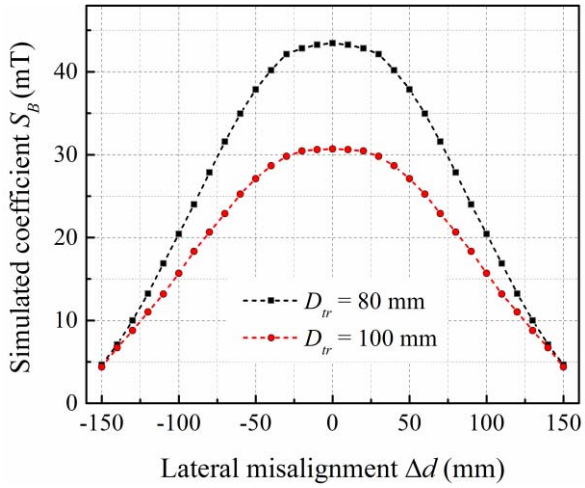

Fig. 6. Simulated coefficient S_B under lateral misalignments.

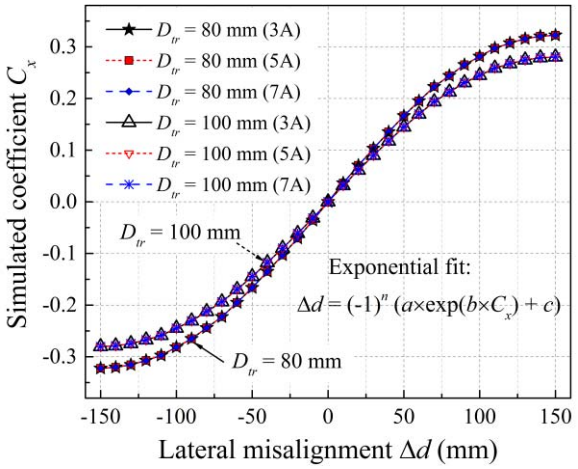

Fig. 8. Relationship between the simulated coefficient C_x and the misalignment Δd along the x-axis direction.

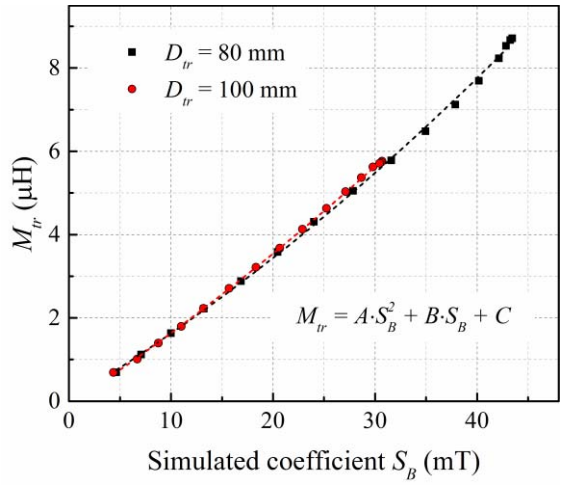

Fig. 7. Simulated M_{tr} versus coefficient S_B in FEM simulations.

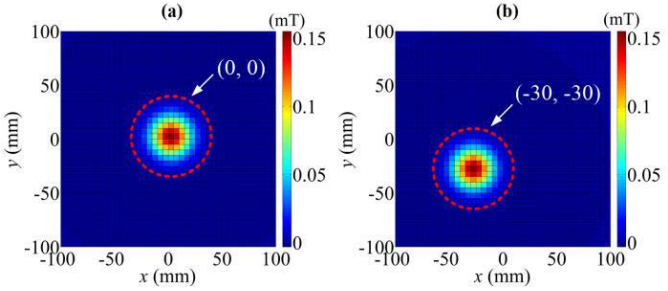

Fig. 9. Simulated magnetic field distributions with metal object at two positions: (a) $x = 0$ mm, $y = 0$ mm and (b) $x = -30$ mm, $y = -30$ mm.

the magnetic strength and size of the metal object. Thus, it is feasible to detect the metal objects from the magnetic field offset measured by a TMR sensor matrix.

IV. Experiments

A. TMR Sensor Matrix and Experimental Platform

In order to validate the proposed approach, a sensor matrix composed of 14 × 14 uniaxial TMR sensor (TMR2001, MultiDimension Technology) was developed to measure the magnetic flux distribution below the receiving coils. Fig. 10 shows the schematic diagram of the TMR-sensor-matrix measurement scheme. The TMR sensors were uniformly distributed as 14 × 14 sensor array on a PCB to constitute a TMR sensor matrix. The distance between the adjacent sensors is 15 mm. The sensors were mounted vertically by a holder that was manufactured using 3D printing technology in order to measure the z-component of magnetic field. It is worth to note that the sensor matrix size and the number of sensors are determined by the size of transmitter and receiver and the requirement of spatial resolution for the magnetic field measurement. Higher spatial resolution requires more sensors which increase the cost and power consumption.

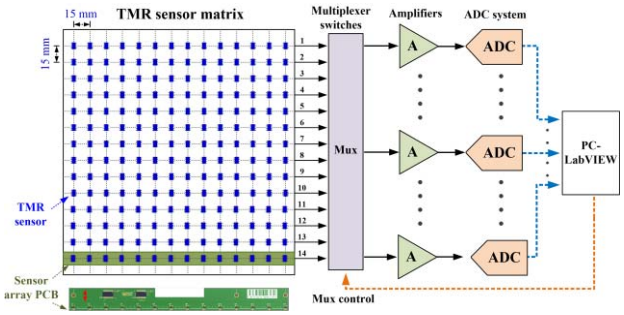

Fig. 10. Schematic diagram of TMR sensor matrix measurement scheme.

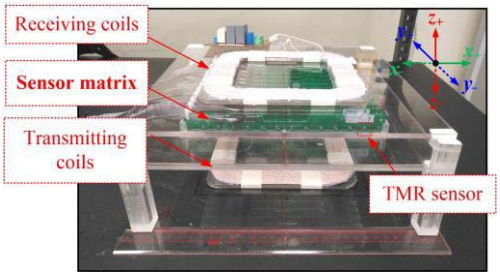

Fig. 11. Photograph of the TMR sensor matrix and coupled coils in WPT.

In this work, the 14×14 sensor array provided magnetic field measurement with sufficient accuracy.

The outputs of the TMR sensor matrix were multiplexed by the 14-channel differential multiplexers (ADG1606, Analog Devices) and then amplified 50 times by the instrument amplifiers (AD620, Analog Devices). By continuously sampling the amplified sensor signals with a sampling rate of 5 MHz, the magnetic flux distribution can be captured and displayed dynamically through the LabVIEW interface.

The WPT prototype was established according to the simulation parameters in Table I. Both transmitting and receiving coils were made of Litz wire to reduce the proximity effect and skin effect. The TMR sensor matrix was placed below the receiving coil (see Fig. 11). The center of the sensor matrix remained well aligned with the receiving coil during experiments. The vertical distance between the sensor matrix and receiving coil was 20 mm. The experimental setup is shown in Fig. 12. The TMR sensor matrix was powered by a constant voltage source (PWS2326, Tektronix). The AC power source was provided by a constant current power supply (PBZ40-10, Kikusui). The control signals to the multiplexers were given by a data acquicition (DAQ) device. Both the currents though the transmitting and receiving coils were measured using two wideband current probes (TCPA300, Tektronix).

B. Calibration of Sensor Matrix

In order to precisely measure the vector magnetic field between the transmitting and receiving coils, the output-field transfer curve of each sensor unit in the TMR sensor matrix was pre-calibrated to eliminate the slight variation of each TMR sensor [24]. During the pre-calibration process, each sensor unit was placed in the center of a programmable 3-axis Helmholtz coil (DXMC15-50, Dexing Magnet) that

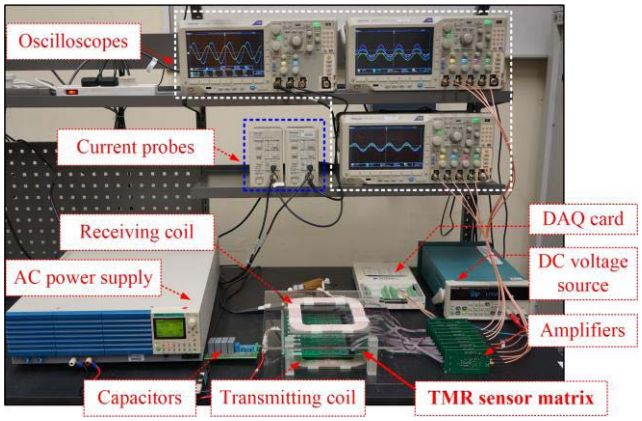

Fig. 12. Experimental setup demonstrating multi-purpose TMR sensor matrix for WPT system.

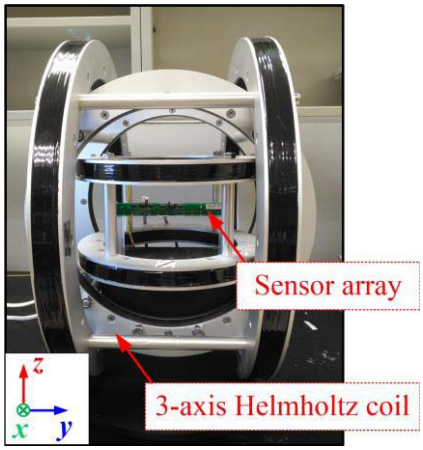

Fig. 13. Calibration of the TMR sensor using a programmable Helmholtz coil.

generates a pre-determined vector magnetic field, as shown in Fig. 13. A precise 3-channel DSP Gaussmeter (Model 460, Lakeshore) with accuracy of $\pm 0.1\%$ was used as the reference. By providing a magnetic field loop, the output-field transfer curve of each TMR sensor was characterized.

The TMR2001 sensors were employed in this work due to their multiple advantages such as compact size (3 mm $\times$ 3 mm $\times$ 1.45 mm), high sensitivity (80 mV/V/mT), wide dynamic range (up to 1 MHz), low cost and excellent thermal stability [25]. Fig. 14 shows the typical output-field transfer curve when the TMR2001 sensor was powered by a constant voltage supply.

This sensor can operate in the linear magnetic field range of ± 1.5 mT. The actual sensor output (V_{out}) of each TMR sensor can be expressed as:

$$V_{out} = V_c(S_t \cdot B \cdot F_s + O_b) \tag{12}$$

where V_c is the constant supply voltage, S_t is the sensor target sensitivity (i.e., 80 mV/V/mT), B is the magnetic flux density to be measured, F_s is the sensitivity scale factor, O_b is the offset voltage. For each sensor of the sensor matrix, the parameters of F_s and O_b need to be determined during the pre-calibration process. All parameters of F_s and O_b were

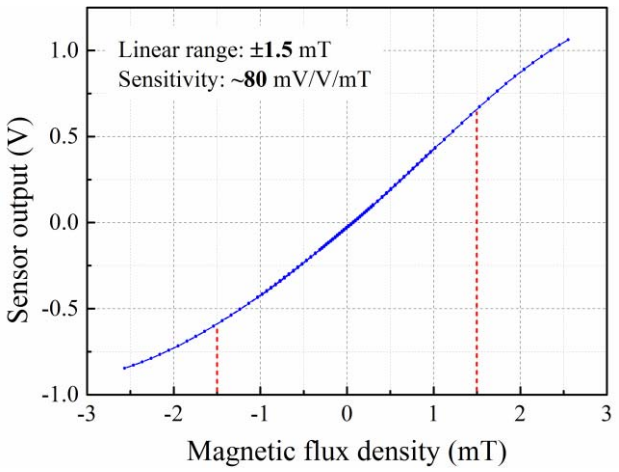

Fig. 14. Typical characteristic output-field transfer curve of TMR2001 sensor at 2 V voltage supply.

stored in a look-up table to ensure precise and consistent magnetic field measurements.

V. Experimental Results and Discussion

The experimental results are presented in this section to validate the proposed approach. When power was wirelessly transferred from the transmitter to the receiver, the magnetic field distribution was measured by the TMR sensor matrix. Fig. 15(a) shows the AC output signals of a sensor array (A7 in Fig. 10) with 14 TMR sensors during the IPT-based WPT operation when the transmitting and receiving coils were well aligned. The TMR sensors generated the sinusoidal voltage signals with frequency of 20 kHz that corresponds to the time-varying magnetic field generated from the WPT operation. Thus, according to Eq. 12 and the obtained parameters of F_s and O_b, the magnetic flux densities in RMS value can be precisely obtained as shown in Fig. 15(b).

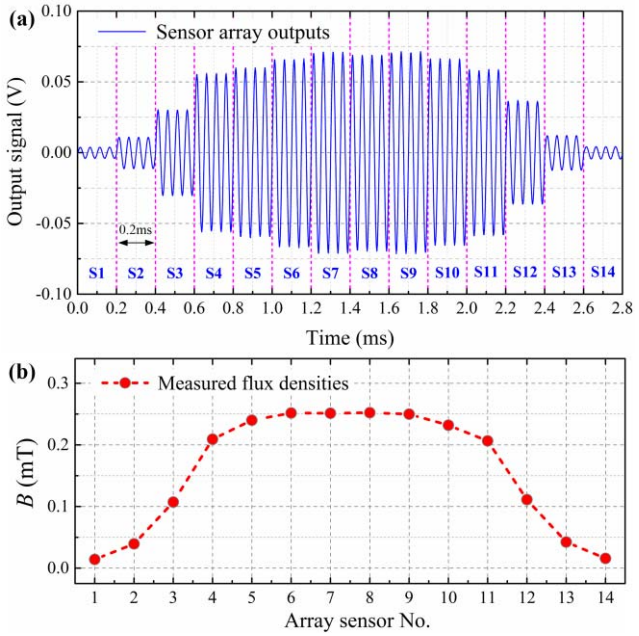

Fig. 15. (a) AC output signal of a TMR sensor array. (b) Measured magnetic flux densities (RMS value) by the sensor array after pre-calibration process.

A. Charging Performance Monitoring

By regulating the misalignment distance Δd along the x-axis direction, the corresponding current waveforms through the transmitting and receiving coils and the magnetic flux density distributions were measured by the current probes and TMR sensor matrix, respectively. Fig. 16 depicts the measured current waveforms and magnetic flux density distributions of the WPT model with vertical distance (d_{tr}) of 80 mm. The current (I_t) through the transmitting coil remained constant during the WPT operation, whereas the current through the receiving coil (I_r) gradually reduced as the misalignment distance increased, which resulted in the gradual decrease of charging power. When the receiving coil was well aligned with the transmitting coil (i.e., $\Delta d = 0$ mm), the magnetic flux concentrated at the center of flux plane. When there existed a misalignment, the concentration of magnetic flux shifted in response to the misalignment.

The relationship between the mutual inductance (M_{tr}) and the coefficient S_B was investigated in experiments. Fig. 17 shows the measured coefficient S_B of the WPT models with two vertical distances (i.e., 80 mm and 100 mm) under lateral misalignments. The measured results of S_B well matched with the simulation results in Fig. 6. S_B reached its maximum value when the coils were well aligned, and then gradually decreased as the misalignment increased. A second-order polynomial fit can be applied to express the relationship between M_{tr} and S_B(see Fig. 7). Thus, M_{tr} can be obtained by the measured S_B as shown in Fig. 18. The measured values of M_{tr} by the TMR sensor matrix well matched with the measured M_{tr} using the LCR meter (LCR-821, ISO-TECH). Thus, it is feasible to measure the mutual inductance of two parallel coupled coils in LPT-based WPT operations by the measured coefficient S_B.

Consequently, the transferred power (P_L) can also be obtained by the measured M_{tr}. As the current source (I_t), resonance frequency (ω) and load resistance (R_L) were kept constant, there existed a second-order polynomial relationship between P_L and M_{tr} according to Eq. (3). The charging power can then be determined as shown in Fig. 19. The charging power measured by the TMR sensor matrix agreed with those measured by the current probe. The measuring errors using the sensor matrix are less than 0.81 W. Thus, this method provides a convenient alternative of charging power monitoring.

B. Coil-Misalignment Detection

The coil misalignment distance and orientation can be detected by the measured symmetry coefficients. Fig. 19 shows the measured coefficients C_x of the WPT models with two vertical distances (i.e., 80 mm and 100 mm) under lateral misalignments along the x-axis direction. The measured coefficient C_x showed the similar pattern as the simulation results (see Fig. 8). Using the exponential fitting model in Fig. 8, the misalignment can be detected using the measured

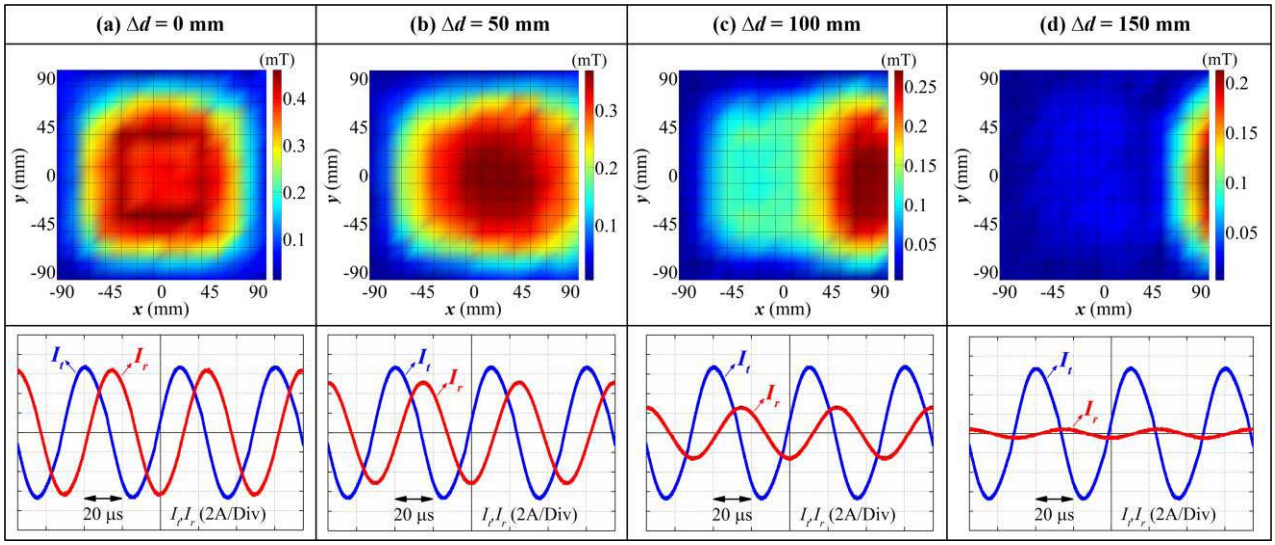

Fig. 16. Measured flux density distributions (RMS value) and current waveforms under different lateral coil misalignments.

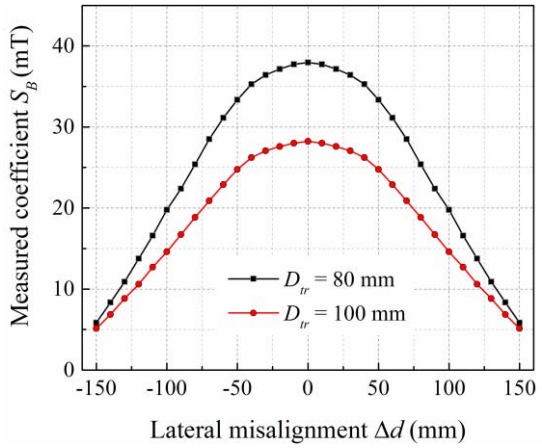

Fig. 17. Measured coefficient S_B by TMR sensor matrix.

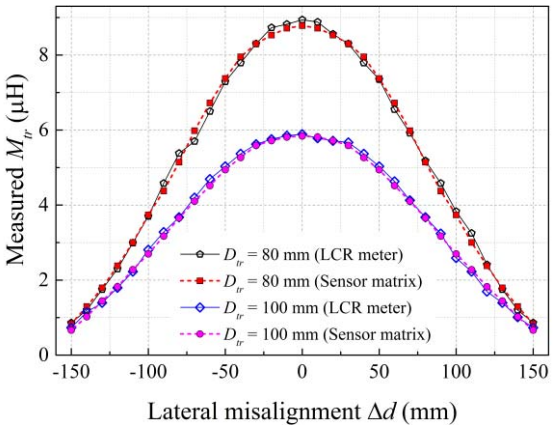

Fig. 18. Measured M_{tr} using the measured coefficient S_B in Fig. 17.

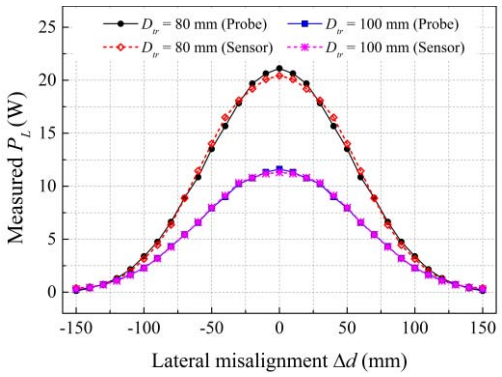

Fig. 19. Measured P_L using the measured coefficient M_{tr} in Fig. 18.

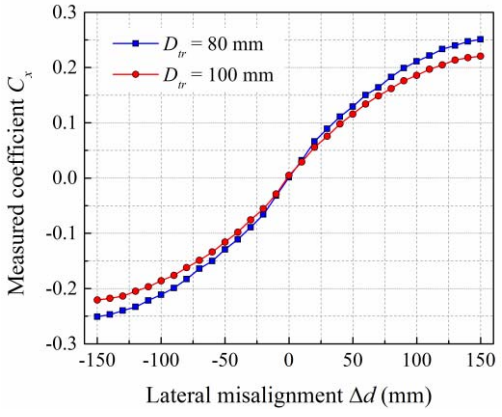

Fig. 20. Measured coefficient C_x under lateral misalignments.

coefficient C_x, as depicted in Fig. 21. The misalignment distance measured by the TMR sensor matrix can match with the actual values in the measurement range of ±150 mm with a measuring error of less than ±3.7 mm. Similarly, the TMR sensor matrix can detect the coil misalignment along both x-axis and y-axis directions.

C. Foreign Metal Object Detection

The TMR sensor matrix is capable of detecting the foreign metal object by measuring the magnetic field offsets. In experiments, a metal object (bolt) shown in Fig. 22 was

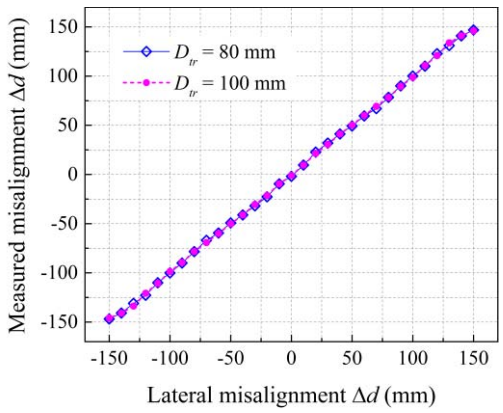

Fig. 21. Measured misalignment by the TMR sensor matrix.

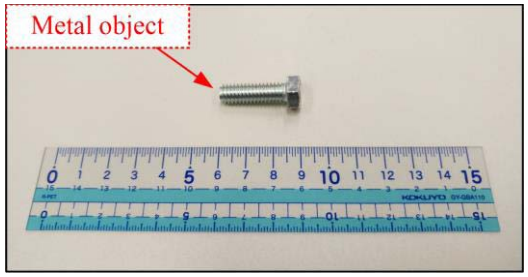

Fig. 22. The metal object detected in experiments.

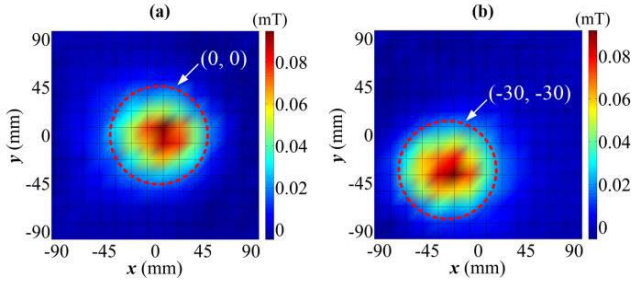

Fig. 23. Measured DC field distributions with the metal object at two positions (a) $x = 0$ mm, $y = 0$ mm and (b) $x = -30$ mm, $y = -30$ mm.

placed over the transmitting coil at the positions of (0 mm, 0 mm) and (−30 mm, −30 mm), respectively. The generated magnetic fields by the metal object in two cases were measured by the TMR sensor matrix, as illustrated in Fig. 23, respectively. There were large magnetic field offsets at the positon corresponding to the location of metal object, which matched with the simulation results in Fig. 9. The generated magnetic field offset (B_{mo}) measured by the TMR sensors reached 0.08 mT. Hence, the metal object can be accurately distinguished by the region of large field offsets (see red circle in Fig. 23). It is worthy to note that the TMR sensor matrix can distinguish more than one metal objects at different locations simultaneously.

VI. Conclusion

In this work, a multi-purpose TMR sensor matrix approach was proposed to monitor the charging performance of wireless EV charging and detect both the existence of coil misalignment and foreign metal objects. This easy-to-installation and cost-effective approach provides a convenient and reliable solution to achieve multiple purposes based on magnetic-filed sensing using a TMR sensor matrix. The overall cost of the TMR sensor matrix is reducing rapidly due to the fast development of TMR technology. Furthermore, the TMR sensor matrix approach has the promising potential to be used in multiple WPT topologies for both stationary and dynamic EV wireless charging.

The future work will focus on the practical implementation issues of wireless EV charging with the TMR sensor matrix technique. The estimation of power transfer efficiency and 3D positioning of receiving coils will be studied. The calculation of power transfer power efficiency under varied working conditions such as variable-current transmitter and variable-resistance battery load will be investigated. The misalignment-tolerant wireless charging technique can be developed with 3D positioning of receiving coils. In addition, the power supply for the sensor matrix module and embedded digital signal processing will also be designed and developed for the practical EV charging applications.

References

[1] L. Xie, Y. Shi, Y. T. Hou, and W. Lou, "Wireless power transfer and applications to sensor networks," *IEEE Wireless Commun.*, vol. 20, no. 4, pp. 140–145, Aug. 2013.

[2] C. Jiang, K. T. Chau, C. Liu, and C. H. T. Lee, "An overview of resonant circuits for wireless power transfer," *Energies*, vol. 10, no. 7, p. 894, Jun. 2017.

[3] Z. Bi, T. Kan, C. C. Mi, Y. Zhang, Z. Zhao, and G. A. Keoleian, "A review of wireless power transfer for electric vehicles: Prospects to enhance sustainable mobility," *Appl. Energy*, vol. 179, pp. 413–425, Oct. 2016.

[4] Q. Zhu, L. Wang, and C. Liao, "Compensate capacitor optimization for kilowatt-level magnetically resonant wireless charging system," *IEEE Trans. Ind. Electron.*, vol. 61, no. 12, pp. 6758–6768, Dec. 2014.

[5] Z. Zhang, K. T. Chau, C. Liu, F. Li, and T. W. Ching, "Quantitative analysis of mutual inductance for optimal wireless power transfer via magnetic resonant coupling," *IEEE Trans. Magn.*, vol. 50, no. 11, Nov. 2014, Art. no. 8600504.

[6] J. P. W. Chow, N. Chen, H. S. H. Chung, and L. L. H. Chan, "An investigation into the use of orthogonal winding in loosely coupled link for improving power transfer efficiency under coil misalignment," *IEEE Trans. Power Electron.*, vol. 30, no. 10, pp. 5632–5649, Oct. 2015.

[7] W. Ni *et al.*, "Radio alignment for inductive charging of electric vehicles," *IEEE Trans. Ind. Informat.*, vol. 11, no. 2, pp. 427–440, Apr. 2015.

[8] K. Hwang *et al.*, "Autonomous coil alignment system using fuzzy steering control for electric vehicles with dynamic wireless charging," *Math. Problems Eng.*, vol. 2015, Nov. 2015, Art. no. 205285.

[9] K. Hwang *et al.*, "An autonomous coil alignment system for the dynamic wireless charging of electric vehicles to minimize lateral misalignment," *Energies*, vol. 10, no. 3, p. 315, Mar. 2017.

[10] Y. Gao, C. Duan, A. A. Oliveira, A. Ginart, K. B. Farley, and Z. T. H. Tse, "3-D coil positioning based on magnetic sensing for wireless EV charging," *IEEE Trans. Transport. Electrific.*, vol. 3, no. 3, pp. 578–588, Sep. 2017.

[11] I. Cortes and W.-J. Kim, "Lateral position error reduction using misalignment-sensing coils in inductive power transfer systems," *IEEE/ASME Trans. Mechatronics*, vol. 23, no. 2, pp. 875–882, Apr. 2018.

[12] N. Kuyvenhoven, C. Dean, J. Melton, J. Schwannecke, and A. E. Umenei, "Development of a foreign object detection and analysis method for wireless power systems," in *Proc. IEEE Symp. Product Compliance Eng. Proc. (PSES)*, Oct. 2011, pp. 1–6.

[13] S. Fukuda, H. Nakano, Y. Murayama, T. Murakami, O. Kozakai, and K. Fujimaki, "A novel metal detector using the quality factor of the secondary coil for wireless power transfer systems," in *IEEE MTT-S Int. Microw. Symp. Dig.*, May 2012, pp. 241–244.

[14] P. S. Riehl, "Wireless charging transmitter using capacitive sensing for device detection," Google Patent 0 261 137 A1, Sep. 9, 2016.
[15] S. Y. Jeong, H. G. Kwak, G. C. Jang, S. Y. Choi, and C. T. Rim, "Dual-purpose nonoverlapping coil sets as metal object and vehicle position detections for wireless stationary EV chargers," *IEEE Trans. Power Electron.*, vol. 33, no. 9, pp. 7387–7397, Sep. 2018.
[16] X. Liu, W. Han, C. Liu, and P. W. T. Pong, "Marker-free coil-misalignment detection approach using TMR sensor array for dynamic wireless charging of electric vehicles," *IEEE Trans. Magn.*, vol. 54, no. 11, Nov. 2018, Art. no. 4002305.
[17] R. Weiss, R. Mattheis, and G. Reiss, "Advanced giant magnetoresistance technology for measurement applications," *Meas. Sci. Technol.*, vol. 24, no. 8, p. 082001, 2013.
[18] L. Jogschies *et al.*, "Recent developments of magnetoresistive sensors for industrial applications," *Sensors*, vol. 15, no. 11, pp. 28665–28689, Nov. 2015.
[19] X. Liu, C. Liu, and P. W. T. Pong, "Velocity measurement technique for permanent magnet synchronous motors through external stray magnetic field sensing," *IEEE Sensors J.*, vol. 18, no. 10, pp. 4013–4021, May 2018.
[20] J. Shin *et al.*, "Design and implementation of shaped magnetic-resonance-based wireless power transfer system for roadway-powered moving electric vehicles," *IEEE Trans. Ind. Electron.*, vol. 61, no. 3, pp. 1179–1192, Mar. 2014.
[21] J. Kim *et al.*, "Coil design and shielding methods for a magnetic resonant wireless power transfer system," *Proc. IEEE*, vol. 101, no. 6, pp. 1332–1342, Jun. 2013.
[22] K. Fotopoulou and B. W. Flynn, "Wireless power transfer in loosely coupled links: Coil misalignment model," *IEEE Trans. Magn.*, vol. 47, no. 2, pp. 416–430, Feb. 2011.
[23] X. Mou, O. Groling, and H. Sun, "Energy-efficient and adaptive design for wireless power transfer in electric vehicles," *IEEE Trans. Ind. Electron.*, vol. 64, no. 9, pp. 7250–7260, Sep. 2017.
[24] F. Xie, R. Weiss, and R. Weigel, "Simple mathematical operation-based calibration method for giant magnetoresistive current sensor applying B-spline modeling," *IEEE Sensors J.*, vol. 16, no. 12, pp. 4733–4739, Jun. 2016.
[25] *TMR2001 TMR Linear Sensor Datasheet*. Accessed: Jul. 2018. [Online]. Available: http://www.dowaytech.com/en/1944.html

Xuyang Liu (S'16) received the B.Eng. degree from the University of Electronic Science and Technology of China, Chengdu, China, in 2015. He is currently pursuing the Ph.D. degree with the Department of Electrical and Electronic Engineering, The University of Hong Kong, Hong Kong. His current research interests include nondestructive testing, advanced sensing technologies, and applications of magnetoresistive magnetic field sensors in electric vehicles and wireless power transfer.

Chunhua Liu (M'10–SM'14) received the B.Eng. and M.Eng. degrees from the Department of Automatic Control, Beijing Institute of Technology, China, in 2002 and 2005, respectively, and the Ph.D. degree from Department of Electrical and Electronic Engineering, The University of Hong Kong, Hong Kong, in 2009. He is currently an Assistant Professor with the School of Energy and Environment, City University of Hong Kong, Hong Kong.

His research interests are in electrical energy and power technology, including electric machines and drives, electric vehicles, electric robotics and ships, renewable energy and microgrid, and wireless power transfer. In these areas, he has published over 130 refereed papers.

Wei Han (S'16) received the B.Eng. degree from Northeastern University, Shenyang, China, in 2014, and the M.Eng. degree from The University of Hong Kong, Hong Kong, in 2015, where he is currently pursuing the Ph.D. degree with the Department of Electrical and Electronic Engineering. His research interests include wireless power transfer techniques, power electronics, and magnetic sensors.

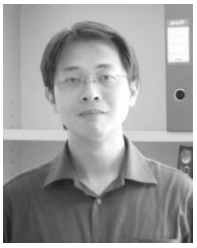

Philip W. T. Pong (SM'13) received the Ph.D. degree in engineering from the University of Cambridge in 2005. He was a Post-Doctoral Researcher at the Magnetic Materials Group, National Institute of Standards and Technology, for three years. In 2008, he joined The University of Hong Kong (HKU) Engineering Faculty, where he is currently an Associate Professor, working on magnetoresistive sensors and their application in smart grid and smart living. He is also a Physicist and Electrical Engineer with the Department of Electrical and Electronic Engineering, HKU, working on magnetoresistive magnetic field sensors and smart grid.